Correcting the propagation of shock waves on uneven meshes with anti-diffusive schemes: application to the 1D Euler equations

R. Chauvin[1], S. Guisset[2], A. Llor[3]
CEA, DAM, DIF F-91297 Arpajon, France

Standard Godunov-type solvers fail in capturing shock waves on uneven meshes: this oft-neglected but serious numerical artifact is produced by the varying numerical viscosity which follows cell size as a shock propagates. This phenomenon and some possible cures are exemplified and studied here for isolated shocks in a simple one dimensional setting. The approaches considered hinge on variants of anti-diffusive Godunov strategies. Numerical results show the effectiveness of the presented conservative anti-diffusive Godunov schemes on strong shock waves propagating over meshes with severe local refinements.

I. Introduction

Common wisdom has it that numerical schemes for hyperbolic set of equations which are consistent, conservative and entropic capture shock waves correctly. In particular, Godunov type schemes based on exact or approximated Riemann solvers [16, 23] are often considered as “the work horse" of computational fluid dynamics: they provide accurate numerical solutions for almost any initial data. However, it is worth noticing that while they are considered to be very robust, Riemann problems based solvers can fail sometimes spectacularly. In [21] a list of possible failures encountered when using Godunov-type schemes is provided. One can mention bad behaviors when studying expansion shocks or slowly moving shocks. In addition, negative internal energies, carbuncle phenomena, kinked mach stems or odd-even decoupling have been

[1] remi.chauvin@cea.fr
[2] sebastien.guisset@cea.fr
[3] antoine.llor@cea.fr

reported [21]. We also mention the works [16, 18, 19] where various numerical artifacts are also encountered and studied.

In this context, the purpose of the present document is twofold. First of all, we intend to point out that a strong numerical artifact arises when propagating a shock wave on a mesh with strong refinements. While it is known, when working with regular solutions, that standard Godunov-type scheme may not be consistent when using uneven meshes, a numerical artifact also occurs when considering the propagation of an isolated shock wave. This drawback was observed by Noh in [20] but remains little known in the computational fluid dynamics community. More precisely, while considering basics Godunov-type strategies for initial conditions leading to isolated shock waves, the numerical diffusion of the schemes produces a non-physical spread of the numerical solutions. The first objective is to point out and explain that, because of this numerical diffusion, all standard Godunov type schemes fails in capturing an isolated shock wave when a strong local refinement is involved.

The second main goal is to show that anti-diffusive-Godunov strategies may be considered and developed to effectively address this issue since no numerical diffusion is involved in the process. In the context of anti-diffusive methods, it is well known that Random-choice type schemes are able to capture sharp interfaces. Concerning the development of Random Choice methods, we refer to the large literature on the subject [7–9, 13, 24] and their references therein for more details. Roughly, the main difference between the standard Godunov type method and the Random choice method is the following: the Godunov method considers an average of local solutions of Riemann problems while the Random Choice pick a single state (a sample) in the local solutions of Riemann problems. Consequently, as demonstrated in [5, 6, 12] they can be adapted to exactly capture isolated shock waves. In the present document, the numerical strategy presented in [5, 12] is considered and extended to obtain a very robust anti-diffusive and conservative Godunov-type scheme which allows the capture of isolated shock waves and overcomes the numerical artifact studied on non-uniform meshes. We also mention that anti-diffusive strategies based on discontinuous reconstruction strategies have also been developed. Originally presented for scalar advection problem, they have been introduced as downwind decentering procedures in [11] and largely studied in [3, 15]. This methodology has then been extended to the numerical capture of contact discontinuities in [2, 10, 17]. More recently, discontinuous reconstruction strategies also emerged for the capture of isolated shock waves [1, 4]. Even if these procedures are not considered herein, we believe they may also be used to develop anti-diffusive schemes to tackle the numerical artifact presented here.

In the present document, we choose to focus on the propagation of shock waves described by the standard compressible Euler equations here given for one-dimensional flow as

$$\begin{cases} \partial_t \rho + \partial_x (\rho u) = 0, \\ \partial_t (\rho u) + \partial_x \left(\rho u^2 + p\right) = 0, \\ \partial_t (\rho e) + \partial_x ((\rho e + p) u) = 0. \end{cases} \tag{1}$$

where ρ, u and ρe are respectively the mass density, velocity, and total energy (sum of internal and kinetic energy). The pressure is denoted p and, by the equation of state, is a nonlinear function of ρ and e. In the following only ideal gas closures are considered

$$p = (\gamma - 1)\rho e, \tag{2}$$

where γ is the adiabatic coefficient. We emphasize that despite the simplicity of this present example, the set of equations (1) constitutes the backbone of a very large variety of more sophisticated models. Consequently, if the numerical artifact already arises in this simple setting, it will certainly also be clearly visible dealing with more complex ones. This motivates a deep understanding of the artifact occurring here and the development of associated numerical strategies to address this issue.

The paper is organized as follows. The first section starts with some numerical observations where the propagation of an isolated shock wave is displayed working on a mesh with a strong local refinement. The numerical artifact is clearly visible. An explanation on the link between the numerical diffusion and the possible loss of the discrete Rankine-Hugoniot conditions is then provided. The second section is devoted to the development and the comparison of several anti-diffusive strategies. In the third and last section it is shown that the last hybrid-Godunov anti-diffusive scheme developed in section two, overcomes the second Noh artifact while remaining robust. This is not the case with the others anti-diffusive schemes when very strong shock waves are involved. Our conclusions, discussions and perspectives are finally given.

II. Failure of standard Godunov schemes on meshes with local refinements.

We start this section by pointing out an important drawback encountered when using standard Godunov type schemes on 1D meshes with localized refinements. More precisely, it is observed that wrong numerical shock wave profiles are obtained when using uneven meshes.

A. Numerical illustrations and context

1. Euler equations

In order to illustrate the present numerical artifact we are going to study, the well-known Noh test case [20] is considered. Here, a strong shock wave is created and propagates with a positive velocity. The initial conditions are the following

$$\begin{cases} \rho(t=0,x) = 1, \\ u(t=0,x) = -1, \\ \rho e(t=0,x) = 0.5 + 1.5 \cdot 10^{-10}, \end{cases} \tag{3}$$

and the adiabatic coefficient $\gamma = 5/3$ such that the initial pressure is 10^{-10} in the domain. The number of cells chosen is 150 and the solution is displayed at time $t = 0.9$. On Figure 1, the density profile around the shock wave is displayed. In the case of a regular mesh (results in red) it is observed that the Rusanov scheme (in dashed line) and the HLL scheme [14], correctly capture the shock propagation. On the contrary, working with the mesh with a local refinement (results in green), one clearly observes a strong numerical artifact with both Rusanov and HLL schemes. For this numerical test case, we have set $\Delta x_{i+1}/\Delta x_i = r$ with $r = 0.9$ (for $x < 0.20$) and $r = 1/0.9$ (for $x > 0.20$). For this mesh, it is observed that once the shock

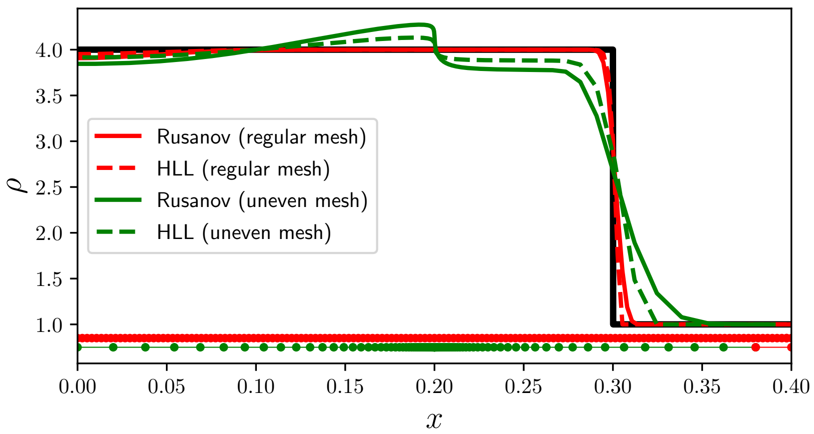

Fig. 1 Numerical shock profiles obtained with a regular mesh (in red) and a mesh with local refinement (in green). Here we have set $\Delta x_{i+1}/\Delta x_i = r$ with $r = 0.9$ (for $x < 0.20$) and $r = 1/0.9$ (for $x > 0.20$).

wave has passed the refinement a numerical artifact is clearly visible. Obviously, the two Godunov schemes do not capture the correct plateau. This wrong behavior may have serious practical consequences. As a matter of fact, when considering realistic applications, if one chooses to increase the refinement of the mesh in a specific area of interest (in which an isolated shock wave will propagate), then, wrong shock profiles will be obtained (despite paying the price of a refined mesh). In the case of regular solutions, it is known that standard schemes are not consistent when using meshes with local refinement. Indeed, a direct look at the associated modified equations working with this type of mesh points out a consistency issue. However, this analysis does not hold when considering non-regular solution profiles and the diagnostic is not clear. All in all, this numerical example highlights a wrong numerical behavior of standard schemes even when working with simple isolated discontinuities. This numerical artifact has already been observed and reported by Noh in [20]. In Figure 2 and 3, the density profiles provided in [20] are recalled. The physical test case considered consists in the propagation of a fluid against a wall (left boundary) so that a right-going shock wave is created. Noh reported two numerical artifacts denoted Type$\#1$ error and Type$\#2$ error on Figure 2 and 3. The Type$\#1$ error is now well-known as the "wall-heating" phenomenon. In addition, Noh also remarked that when artificially "freezing" the characteristic length in the artificial-viscosity (so the length of the shock wave) injected into the scheme, the Type$\#2$ error vanishes (see Figure 3). Of course such a strategy can not be used in practice since it leads to a loss of the advantages of locally refined meshes. In the following the numerical artifact depicted on Figure 1 will be called “the second Noh artifact" in reference to the Type$\#2$ error reported by Noh.

2. *Others set of equations*

It has been checked if the second Noh artifact studied here also shows up when working with others well-known set of equations. Here the results obtained using the Burger equation and the barotropic Euler equations are presented. In Figure 4 solution profiles have been displayed working with the well-known Burger equation. The initial profile is displayed in red while the exact solution is in black and the numerical solution in green. The final time is set so that the discontinuity propagates through the strong local refinement. We have set a strong local refinement taking $r = 0.6$ for $x < 0.125$ and $r = 1/0.6$ for $x < 0.125$. It is clearly observed that despite the strong refinement no numerical artifact occurs here. Similar numerical tests

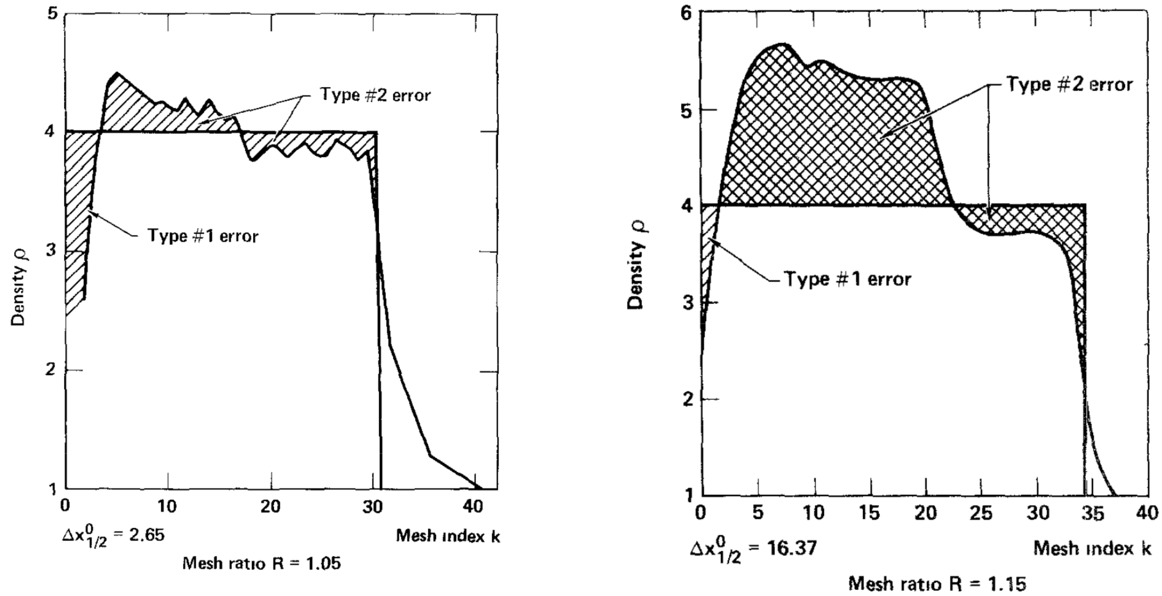

Fig. 2 Density profiles reported by Noh [20]. The Type$\#1$ error is now well-known as the "wall-heating" phenomenon while the Type $\#2$ error is due to the use of a non regular mesh.

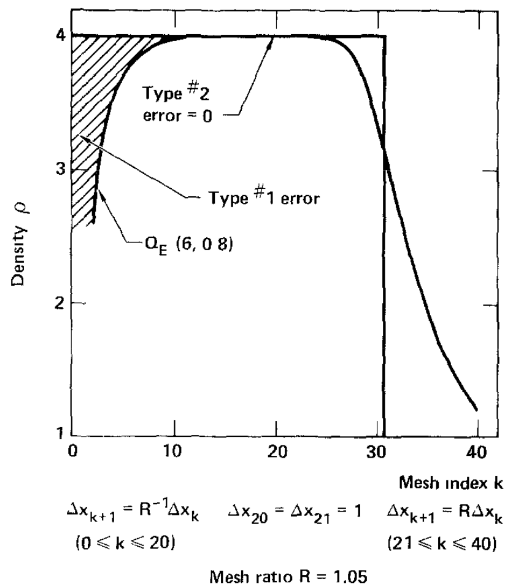

Fig. 3 Density profile reported by Noh [20]. When considering a constant characteristic length in the artificial viscosity of the scheme, the Type $\#2$ error vanishes.

have also been carried out working with the barotropic Euler equations. In Figures 5-6-7 density profiles have been displayed working with the barotropic Euler equations at different times so that the shock wave propagate through the mesh refinement (here we chose $r = 0.2$). In Figure 6 at time $t = 3.7$ a numerical artifact is clearly visible. Looking at the density profile at time $t = 4$ with Figure 7, one understands that the numerical propagates and is damped by the numerical viscosity of the scheme. For comparison, the results obtained working with the full Euler equations are displayed in Figures 8-9-10 (here we chose $r = 0.2$). Looking at Figure 9 and Figure 10 two numerical are visible. The first one remains located on the mesh refinement and corresponds to the second Noh artifact studied here while the second one propagates and is damped similarly to what it is obtained with the barotropic equations.

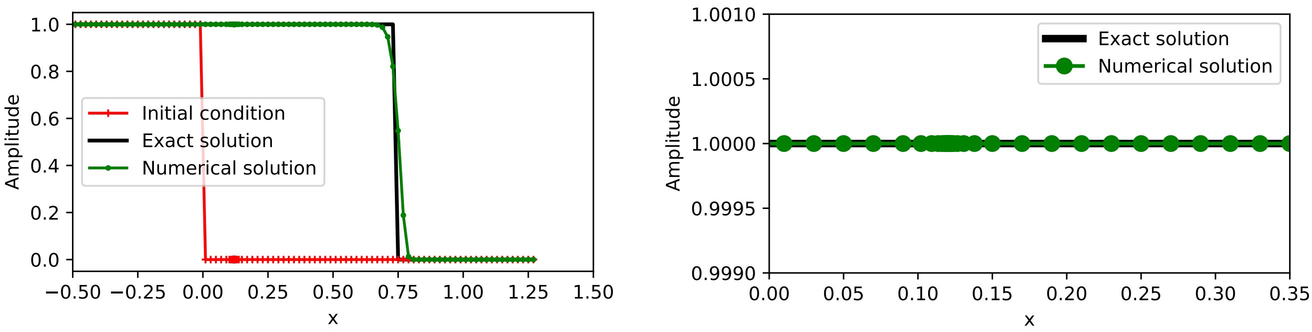

Fig. 4 Solution profiles obtained working with the Burger equation. Despite the strong mesh refinement, the numerical artifact does not appear.

B. Discrete Rankine–Hugoniot conditions

Since the solution profiles studied are not regular, standard consistency analysis does not hold and another approach is then required to explain the second Noh artifact. In this section, it is explained that the second Noh artifact may be understood as a loss of the discrete Rankine–Hugoniot conditions.

1. Numerical observations

In Figure 11, dimensionless density, momentum and energy profiles taken in the framework of the shock with 200 cells (left) and 400 cells (right) are displayed in the case of an isolated shock wave. More precisely the following quantities, taken in the framework of the shock, are displayed

$$\tilde{q} = \frac{q^R - q}{q^R - q^L}, \qquad q = \rho, \rho u, \rho e \tag{4}$$

where q^L and q^R respectively refer to the left and right states (quantities after and before the shock). Firstly, it is observed that the density and energy profiles do not superimpose exactly. Secondly, as expected when

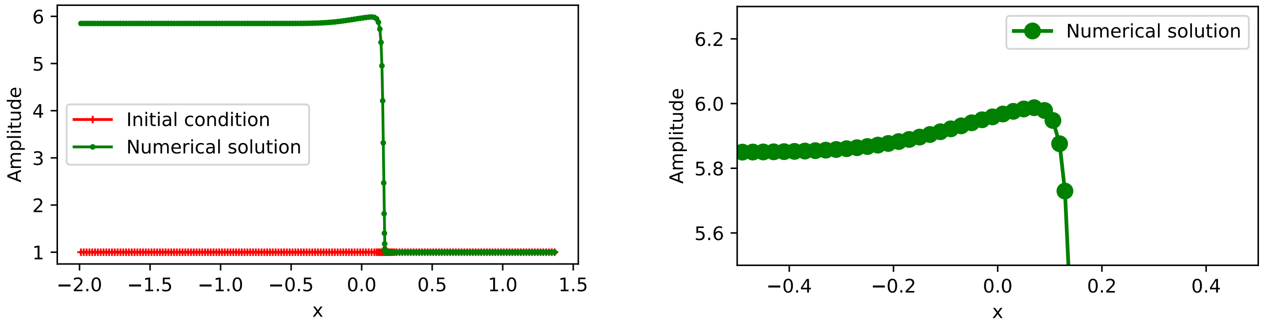

Fig. 5 Density profiles obtained working with the barotropic Euler equations at time $t = 3.5$. The shock wave propagates through the strong refinement.

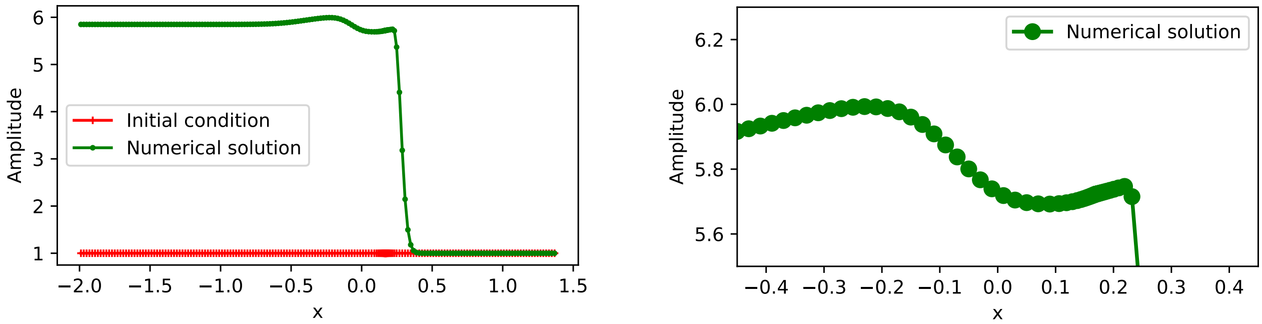

Fig. 6 Density profiles obtained working with the barotropic Euler equations at time $t = 3.7$. A numerical artifact is clearly visible and starts to propagate.

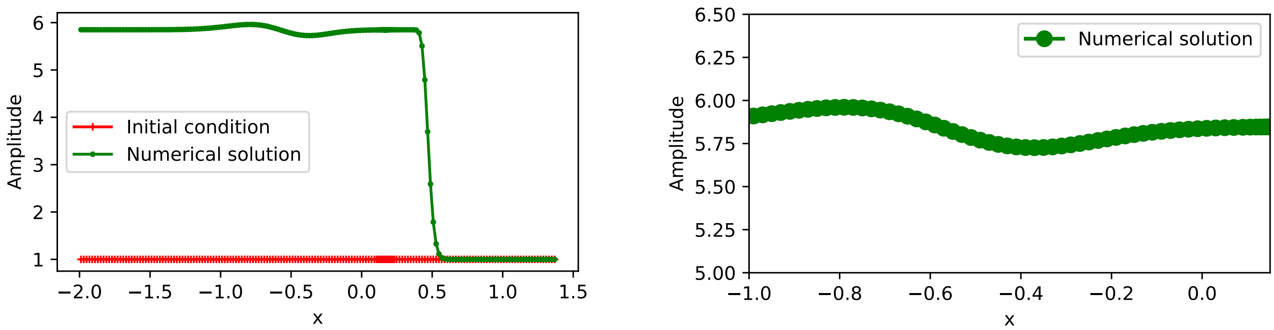

Fig. 7 Density profiles obtained working with the barotropic Euler equations at time $t = 4$. As the numerical artifact propagates it is diffused by the numerical viscosity of the scheme.

using a more refined mesh (Figures from left to right), the shock profiles become sharper. Thirdly, a closer look shows that the mesh refinement also modifies the distance between the shock profiles. Indeed, in Figure 11 (bottom left and right) the red and blue crosses represent the frame origin in which the integral under the curve vanishes (computed numerically). This enables to carefully study the distances between the

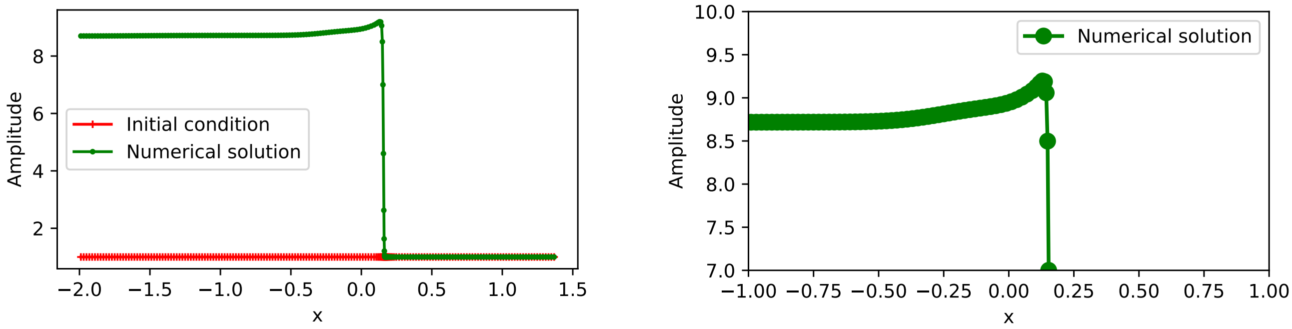

Fig. 8 Density profiles obtained working with the Euler equations at time $t = 5.6$. The shock wave propagates through the strong refinement.

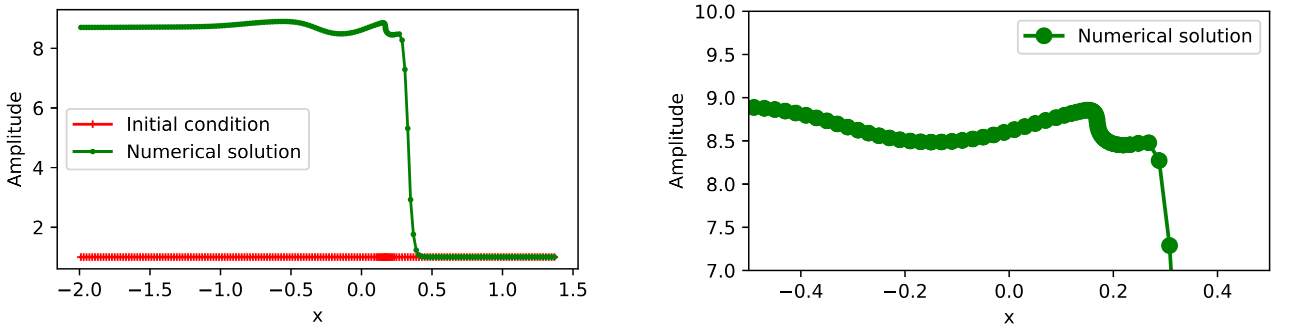

Fig. 9 Density profiles obtained working with the Euler equations at time $t = 6$. Two numerical artifact are clearly visible. One located on the mesh refinement and a second one which starts to propagate (similarly to the one obtained with the barotropic Euler equations).

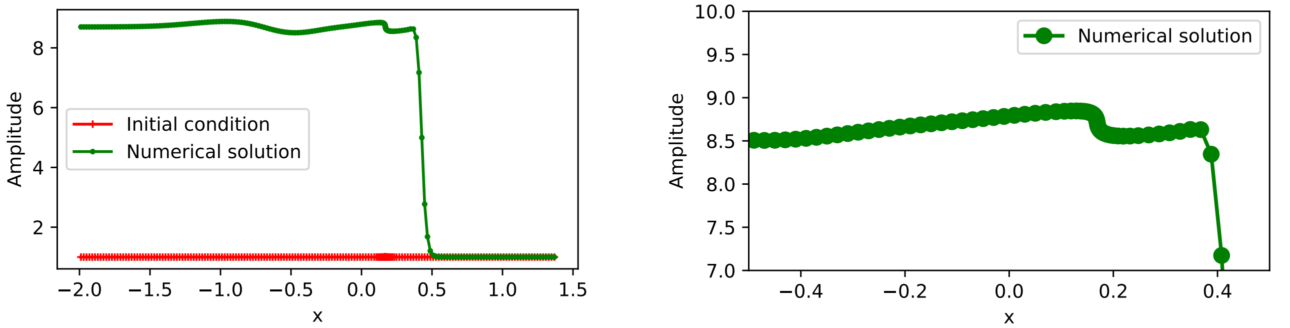

Fig. 10 Density profiles obtained working with the Euler equations at time $t = 6.25$. The first numerical artifact still remains located on the mesh refinement (second Noh artifact). The second continues to propagate and is damped with the numerical viscosity of the scheme.

shock profiles. In particular, it is observed that the red surfaces are not constant when modifying the mesh so the distances between the shock profiles vary.

2. Discrete Rankine–Hugoniot conditions

Let us consider an isolated shock wave traveling with a constant velocity, and the framework moving with respect to the shock speed. By Galilean invariance, the form of the Euler equations is unchanged. Now, the discrete space integration between an abscissa before and after (upstream and downstream) the shock respectively denoted by the index cell i_a and i_b leads to

$$\sum_{i_a}^{i_b}\left(\partial_t U_i + \frac{F_{i+1/2} - F_{i-1/2}}{\Delta x_i}\right)\Delta x_i = \frac{d}{dt}\left(\sum_{i_a}^{i_b} U_i \Delta x_i\right) + F_{i_b+1/2} - F_{i_a-1/2} = 0. \tag{5}$$

In the case of a mesh with a constant space step there is no numerical viscosity variation as the shock wave propagates. Consequently, in this case, the shock profile remains unchanged and it yields

$$F_{i_b+1/2} - F_{i_a-1/2} = 0, \tag{6}$$

such that the discrete Rankine-Hugoniot conditions are ensured (Rankine-Hugoniot conditions in the shock wave framework). On the contrary, in the case of a progressive mesh, because of the change of numerical viscosity, the shock length varies, thus the temporal derivative in (5) does not vanish (variation of the red surfaces in Figure 11) and equation (6) is not recovered. The numerical viscosity of standard Godunov type schemes, which usually give strong stability properties, leads in this case, to the loss of the discrete Rankine-Hugoniot conditions and to the second Noh artifact.

In the previous section it has been observed that no numerical artifact appears when working with the Burger equation. For that scalar equation, the discussion on the discrete Rankine-Hugoniot conditions provides a possible explanation. Indeed, in a case of a simple scalar equation, there always exists a framework in which the integral of the solution vanishes so that the jump relations are correctly recovered. Concerning the numerical results obtained with the barotropic Euler equations, a numerical artifact is clearly visible. It propagates and is damped by the numerical viscosity of the scheme. One could expect to see the second Noh artifact (perturbation which remains located on the local refinement) arises here but it is not so. Contrarily to the full Euler system, the fluid velocity u (here equals to zero after the pass of the shock) is not an eigenvalue of the system. Therefore the perturbation can not maintain itself and propagates.

In order to avoid the numerical artifact one could think in locally modifying the numerical viscosity of the numerical scheme in order to enforce condition (6). However, this point seems particularly challenging while ensuring the stability of the scheme. For this reason, in the next sections, it is shown that anti-diffusive

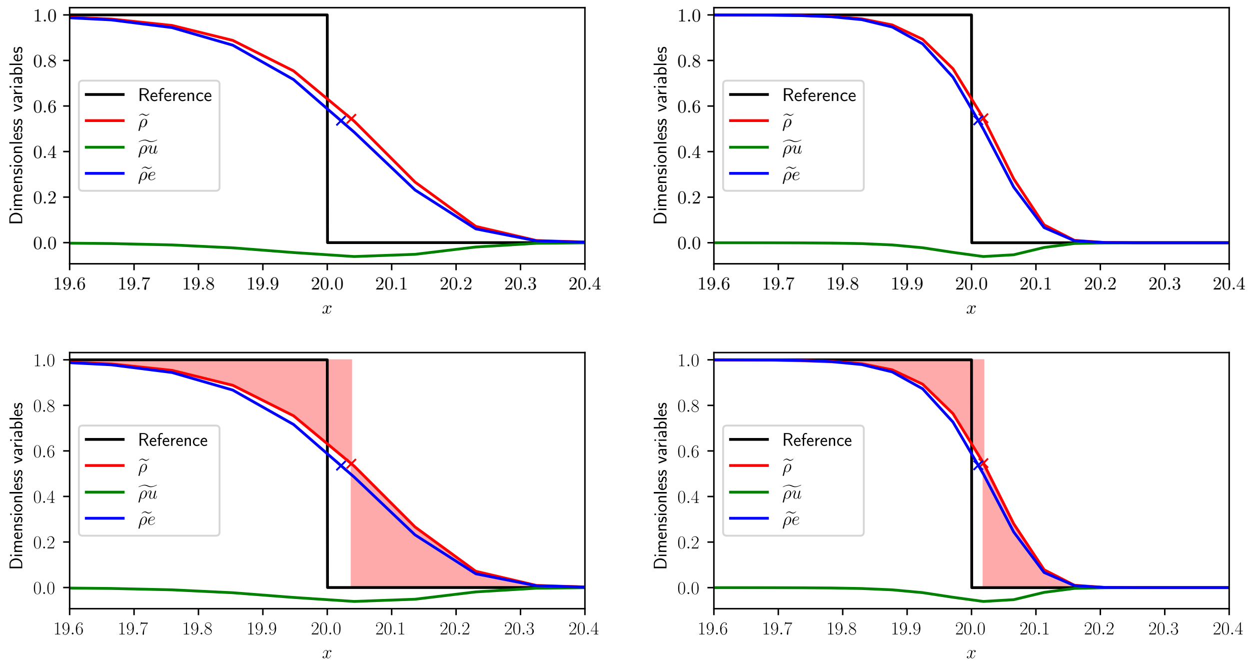

Fig. 11 Dimensionless shock profiles with 2000 cells (left) and 4000 cells (right). The crosses represent the frame origin in which the integral under the curve vanishes (computed numerically).

methods may be used to get rid of the second Noh artifact.

III. Anti-diffusive numerical schemes.

As explained in the previous section, the numerical viscosity variation leads to the second Noh artifact. Several anti-diffusive strategies are now presented.

A. Standard Random Choice Method

1. The Random Choice Method for exact shock capturing

In this section, we briefly recall the Random choice method formalism [24] and applied it to the Euler equations working with a standard HLL numerical scheme. Concerning the development of Random Choice methods, we refer to the large literature on the subject [7–9, 13, 24] and their references therein for more details. Roughly, the main difference between the standard Godunov type method and the Random choice method is the following: the Godunov method considers an average of local solutions of Riemann problems while the Random Choice pick a single state (a sample) in the local solutions of Riemann problems. More precisely, the Random choice method updates the numerical solution in cell i U_i^{n+1} from the solutions U_i^n

of the previous time step, considering the two following steps

Step a. Resolution of a Riemann problem at each interface knowing the numerical solutions U_i^n (step similar to the Godunov method). Exact or approximate Riemann solvers can be considered here. Obviously, if one expects to capture an isolated shock using an approximate Riemann solver, this solver is required to be exact for this problem. For the following, we denote $U^\star$ the solution obtained with the approximate Riemann solver retained. For clarity, we write $U^\star$ as a constant state (HLL intermediate state) but of course it could be made dependent on space and time (general Godunov solver).

Step b (pick up step). The updated numerical solution is picked at random (or quasi-random) as follows

$$U_i^{n+1} = \begin{cases} U^\star_{i-1/2}, & \text{if } 0 \leq \theta^n \leq \lambda_{3,i-1/2}\Delta t/\Delta x, \\ U_i^n, & \text{if } \lambda_{3,i-1/2}\Delta t/\Delta x \leq \theta^n \leq 1 - \lambda_{1,i+1/2}\Delta t/\Delta x, \\ U^\star_{i+1/2}, & \text{if } 1 - \lambda_{1,i+1/2}\Delta t/\Delta x \leq \theta^n \leq 1, \end{cases} \tag{7}$$

where the wave speeds λ_1 and λ_3 are given by the underlying approximate Riemann solver and the parameter θ^n is a chosen at random (or quasi-random) in the interval $[0, 1]$ see Figure 12. It is known [24] that the quality of the numerical method strongly depends on the random numbers θ^n. Following the ideas of [8, 9] the sequence of parameters θ^n is chosen as the Van der Corput Pseudo-Random sequence (low discrepancy sequence) and is computed using the following formulae

$$\theta^n = \sum_{k=0}^{m} i_k 2^{-(k+1)}, \qquad n = \sum_{k=0}^{m} i_k 2^k, \tag{8}$$

where i_k is found by binary expansion of the integer n. We highlight the interest of this approach when considering isolated shock waves. As a matter of fact, during Step a, one may consider a numerical solver which is exact for isolated shocks (it is the case for example for the HLL scheme considering Roe speeds [22] in the case of a perfect gas). Then, during Step b, thanks to the sampling procedure, no numerical diffusion is involved leading to the preservation of the shock profile. This is not the case with the average procedure of the Godunov method.

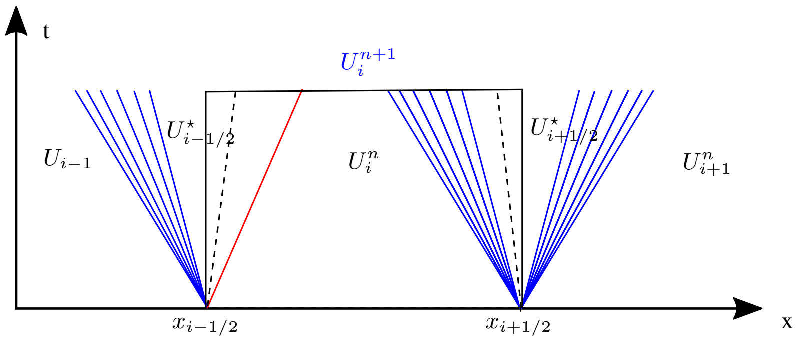

Fig. 12 While the Godunov method considers an average on the cell i to update the solution, the Random choice method picks the solution between the states $U^\star_{i-1/2}$, $U^\star_{i+1/2}$ and U_i^n.

2. Application to the Euler equations with a simple HLL scheme

The methodology presented is now applied to the Euler equations considering a standard approximate HLL Riemann solver with Roe velocities [22]. It is shown that this choice of velocities enables an exact capture of an isolated shock wave.

Step a. An HLL approximate Riemann solver with Roe velocities Consider the most simple approximate Riemann solver made of only one intermediate state $U^\star$, the consistency relations with the integral form of the approximate Riemann solver (Harten, Lax and Van Leer formalism [14]) gives the following definition for the intermediate state $U^\star$

$$U^\star = \frac{\lambda_3 U^R - \lambda_1 U^L - (F(U^R) - F(U^L))}{\lambda_3 - \lambda_1}, \tag{9}$$

where λ_1 and λ_3 are the wave speeds considered in the approximate Riemann solver. While several definitions of λ_1 and λ_3 can be considered, this choice is critical when capturing isolated shock waves. In the present study, following [22] and its applications for anti-diffusive methods [6, 12] we set

$$\lambda_1 = \tilde{u} - \tilde{c}, \qquad \lambda_3 = \tilde{u} + \tilde{c}, \tag{10}$$

where

$$\tilde{u} = \frac{\sqrt{\rho^L} u^L + \sqrt{\rho^R} u^R}{\sqrt{\rho^L} + \sqrt{\rho^R}}, \qquad \tilde{H} = \frac{\sqrt{\rho^L} H^L + \sqrt{\rho^R} H^R}{\sqrt{\rho^L} + \sqrt{\rho^R}}, \qquad \tilde{c} = \sqrt{(\gamma - 1)(\tilde{H} - \tilde{u}^2/2)}.$$

These definitions are obtained by setting a Roe matrix [16, 22] and enables to follow the shock wave exactly in the case of a perfect gas.

Proposition 1. *The HLL approximate solver* (9) *with the Roe velocities* (10) *is exact for an isolated shock wave.*

Proof. Consider an isolated shock wave so we can write the following Rankine-Hugoniot relations

$$\sigma(U^L - U^R) = F(U^L) - F(U^R), \tag{11}$$

where σ denotes the shock velocity and F denotes the physical flux. Now, considering the HLL approximate Riemann solver (9) with the Roe velocities (10) in the case of a 3-shock yields

$$\lambda_3 = \tilde{u} + \tilde{c} = \sigma. \tag{12}$$

The intermediate state (9) rewrites

$$U^\star = \frac{(\tilde{u} + \tilde{c})U^R - (\tilde{u} - \tilde{c})U^L - \sigma(U^R - U^L)}{2\tilde{c}} = U^L.$$

The HLL approximate solver with the Roe velocities (10) is then exact for isolated shock wave. In the case of a 1-shock, the same procedure holds to find $U^\star = U^R$. ☐

Step b (Pick up step). The sampling step is similar to the one described in the previous section, and we refer to equation (7) to update the numerical solution.

Despite its attractive anti-diffusive property, as it will be shown in the next sections, this numerical scheme produces spurious oscillations when strong shocks waves are involved. For this reason, in the next section a more robust anti-diffusive scheme is considered.

B. Hybrid Random-Choice-Godunov method

The anti-diffusive strategy introduced in [6, 12] is presented. This numerical method can be understood as a hybrid method between standard Godunov method and the Random choice method introduced in the previous section. It will be shown in the numerical scheme that the resulting scheme is more robust than the Random choice scheme while preserving the anti-diffusive character.

Step a. Exact approximate Riemann solver for isolated shock waves This step is similar to the one described in the previous section. As explained an HLL solver with Roe velocities may be considered (of course other choices can be made).

Step b. Average step on a new mesh One of the key ingredient of this scheme is the use of a new temporary mesh (virtual mesh). Here the averaging procedure to update the solution of the cell i is not performed on the physical mesh $[x_{i-1/2}, x_{i+1/2}]$ (as with the standard Godunov methods) but on a virtual mesh $[\bar{x}_{i-1/2}, \bar{x}_{i+1/2}]$. The virtual mesh is not uniform, it follows the shock wave and can be defined as

$$\bar{x}^n_{i-1/2} = x_{i-1/2} + \sigma^n_{i-1/2}\Delta t^n,$$

where the speed $\sigma^n_{i-1/2}$ is fixed in order to follow the shock propagation. In Figure 13, the cell $[\bar{x}_{i-1/2}, \bar{x}_{i+1/2}]$ is displayed starting from cell $[x_{i-1/2}, x_{i+1/2}]$ in the case of an isolated shock wave detected at the interface $x_{i-1/2}$ (right-going shock). Of course, in order to move the mesh with the shock wave, a detector method must be used. Now, in the spirit of the Godunov method an average procedure is considered. However, the average step is performed on the virtual mesh instead of the physical mesh. For the next step, the quantities derived on the virtual mesh are denoted $\bar{U}^{n+1}_i$ while the quantities on the physical mesh are denoted U^{n+1}_i.

Step c. Pseudo-random sampling Finally to obtain the updated quantities U^{n+1}_i on the physical mesh (we do not keep the moving virtual mesh), the numerical solution is picked pseudo-randomly among the quantities $\bar{U}^{n+1}_{i+1}$, $\bar{U}^{n+1}_{i-1}$ and $\bar{U}^{n+1}_i$ as follows

$$U^{n+1}_i = \begin{cases} \bar{U}^{n+1}_{i-1} & \text{if} \quad \theta^n \in \Big[0, \dfrac{\Delta t}{\Delta x}\max(\sigma_{i-1/2}, 0)\Big], \\ \bar{U}^{n+1}_{i} & \text{if} \quad \theta^n \in \Big[\dfrac{\Delta t}{\Delta x}\max(\sigma_{i-1/2}, 0), 1 + \dfrac{\Delta t}{\Delta x}\min(\sigma_{i+1/2}, 0)\Big], \\ \bar{U}^{n+1}_{i+1} & \text{if} \quad \theta^n \in \Big[1 + \dfrac{\Delta t}{\Delta x}\min(\sigma_{i+1/2}, 0), 1\Big]. \end{cases}$$

The sampling step is similar to the one presented for the standard Random choice method and the pseudo-random parameter θ^n is also given by (8). As already stated this numerical scheme can be understood as a hybrid method between standard Godunov method and the usual Random choice method. However, one of the key point lies in the clever averaging step. Indeed, thanks to the use of the virtual mesh (which exactly follows the shock wave) no average is performed through a shock (the shock waves are localized at the interfaces of the virtual mesh). Therefore, no numerical diffusion is added in the process. Then, in the spirit of the standard Random choice method, the sampling procedure enables to recover the data on the physical mesh. Before concluding this part, we give the shock detector used in the present work (of course other detectors could be considered). The speed $\sigma_{i+1/2}$ is defined as follows

$$\sigma_{i+1/2} = \begin{cases} \lambda^{n+1}_{i+1/2} & \text{if} \quad u_i > u_{i+1} \ \text{ and } \ \rho_i > \rho_{i+1}, \\ -\lambda^{n+1}_{i+1/2} & \text{if} \quad u_i > u_{i+1} \ \text{ and } \ \rho_i < \rho_{i+1}, \\ 0 & \text{otherwise.} \end{cases}$$

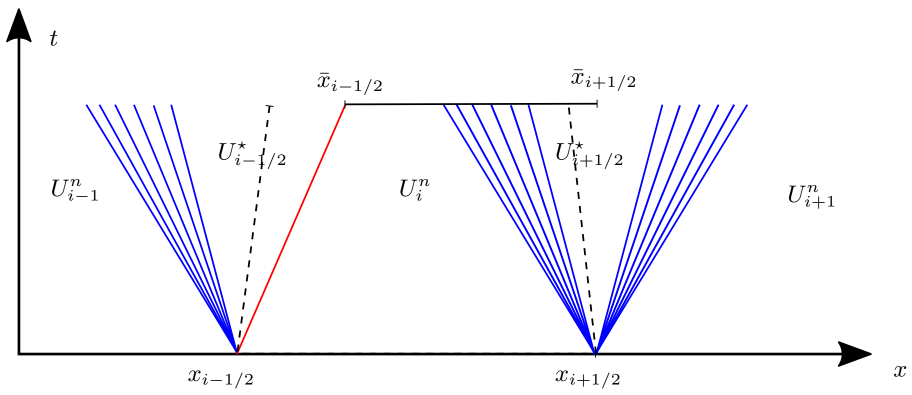

Fig. 13 A new mesh is defined to follow the shock waves. The average step is performed on the virtual mesh instead of the physical mesh.

C. An anti-diffusive and conservative ALE-Godunov scheme (ACA scheme).

The Random choice method (RCM) and the Godunov-Random choice method (RCM-Godunov) presented in the two previous section are not perfectly conservative (there are only conservative in a statistical sense). In addition, while the RCM-Godunov scheme is more robust than the RCM scheme, it will be shown in the numerical section, that the RCM-Godunov scheme still suffers from stability issues in the presence of very strong shock (Noh problem). Therefore, an anti-diffusive, conservative and robust ALE-Godunov scheme is finally presented. This scheme is perfectly conservative, it is anti-diffusive for isolated shock waves and remains stable even in the presence of very strong shocks. The procedure is the following

Step a. Exact approximate Riemann solver for isolated shock waves This step is similar to the one described in detail in the previous section. As explained an HLL solver with Roe velocities may be considered.

Step b. Average step on a new mesh This step is also similar to the one in the previous section. An average step is considered on the new mesh defined to follow the propagation of the shock wave.

Step c. Working with a moving mesh Here, in order to obtain a robust conservative method a different projection technique (no pseudo-random sampling) is considered. In this case we keep working with the virtual mesh which is not virtual anymore. This strategy is clearly conservative since no sampling is used, however as the interfaces move with the shock waves, the size of the cells varies. When the cell size becomes too small a remesh procedure is then used. However, in order to keep the anti-diffusive character of the method, the shock positions are kept during the projection phase. A standard conservative projection is then used. The projection process is illustrated on Figure 14. In this example the shock wave is localized on the interface $x_{i-1/2}$ at time t^n. The shock wave then propagates towards the right side of the domain and it is observed that the size of the i^{th} cell is largely reduced. The solution is then projected keeping the shock position (now interface $x_{i+1/2}$) while the interface $x_{i-1/2}$ is relocated at its initial position. The following conservative projection can be considered

$$\begin{cases} \Delta x_{j+1}^{n+1} U_{j+1}^{n+1} = \Delta \bar{x}_j \bar{U}_j + \Delta \bar{x}_{j+1} \bar{U}_{j+1}, \\ \Delta x_j^{n+1} U_j^{n+1} + \Delta x_{j-1}^{n+1} U_{j-1}^{n+1} = \Delta \bar{x}_{j-1} \bar{U}_{j-1}. \end{cases}$$

Here we choose $U_j^{n+1} = U_{j+1}^{n+1}$ so the solution at time t^{n+1} is completely determined. Again, the key ingredient to obtain the anti-diffusive character is to consider no average through the shock waves. In the next section , it will be shown (with several test cases) that this method is anti-diffusive, conservative and robust.

IV. Numerical results

Different numerical tests are presented demonstrating the interest in using anti-diffusive strategies when progressive meshes are involved.

A. Isolated weak shock wave

The first numerical test case we consider consists in the propagation of a weak shock wave. At the initial time the fluid propagates with a negative velocity, and we enforce a wall boundary condition on the

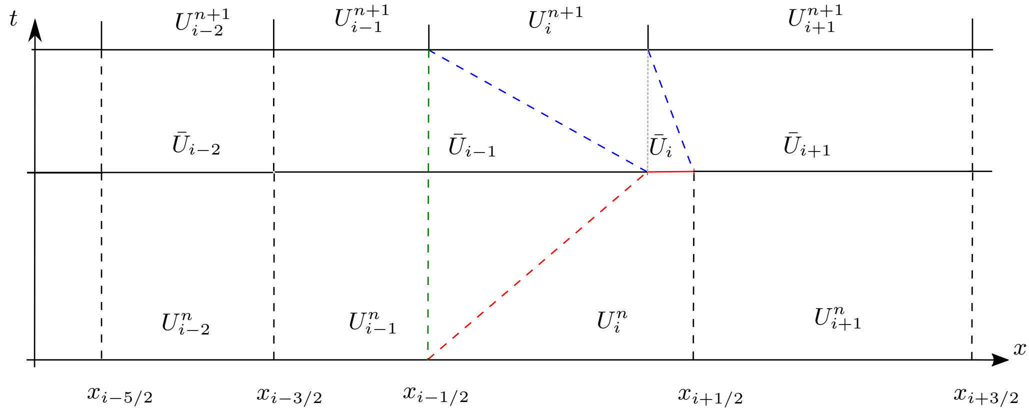

Fig. 14 Working with a moving mesh: the mesh follows the shock wave. When the cells size becomes too small the solution is projected on a new regular mesh keeping the shock position (anti-diffusive property).

left boundary so that a right-going shock wave is created. The initial conditions are the following

$$\begin{cases} \rho(t=0,x) = 1, \\ u(t=0,x) = -1, \\ \rho e(t=0,x) = 2. \end{cases}$$

The space domain is $[0, 0.3]$, the number of cell is 100 and the time step is $t = 0.1786$ (the final time is set so that the shock wave reaches $x = 0.2$). The number of cells is 100 and $\gamma = 5/3$. The results obtained with the Random-Choice scheme (denoted RCM), the hybrid Random-Choice-Godunov scheme (denoted RCM-Godunov), the anti-diffusive and conservative ALE scheme (denoted ACA) and a HLL scheme are compared.

a. Case of a regular mesh (no geometric progression)

We start showing the numerical results obtained when using a regular mesh. Figures 15, 16 and 17 display the density, momentum and energy profiles at the final time. As expected the HLL scheme is diffusive while all the anti-diffusive schemes allow the solution profiles to remain sharp around the shock waves. This already shows the interest in using anti-diffusive strategies when studying the propagation of shock waves. In Figure 18, the global density and momentum conservations in the domain are displayed as function of time. As expected the HLL scheme and the ACA scheme are perfectly conservative while the RCM and RCM-Godunov scheme are only conservative in a statistical sense.

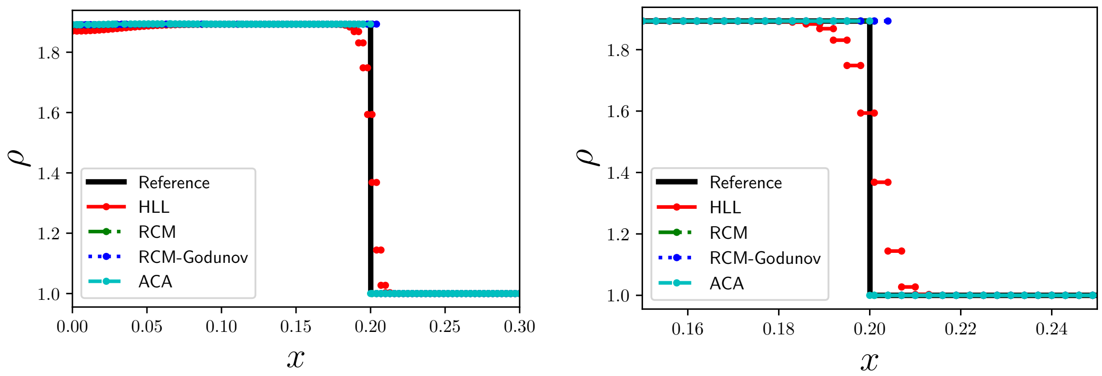

Fig. 15 Isolated weak shock wave: density profile (left) and zoom on the right going shock (right).

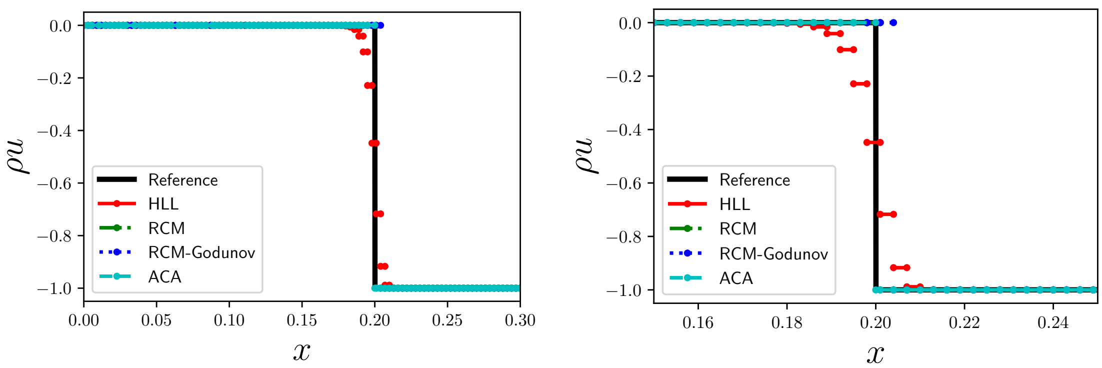

Fig. 16 Isolated weak shock wave: momentum profile (left) and zoom on the right going shock (right).

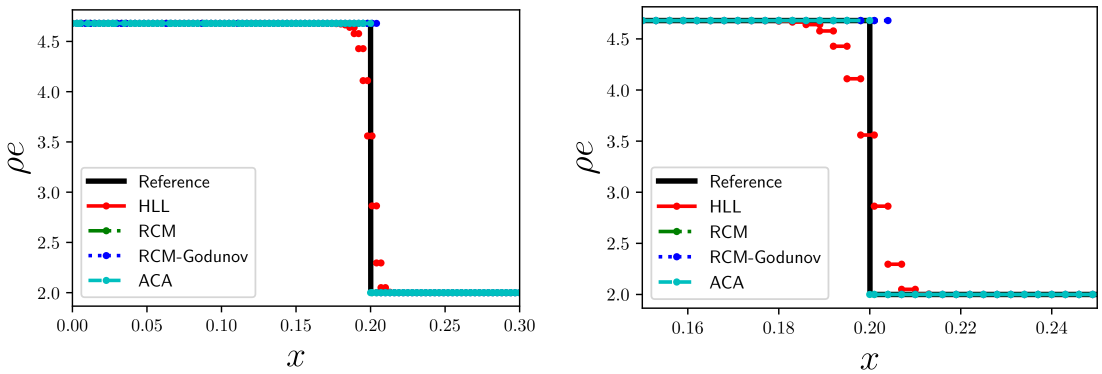

Fig. 17 Isolated weak shock wave: total energy profile (left) and zoom on the shock (right).

b. Case of a mesh with local refinement

The same test case is now studied working with a progressive mesh. For this test we set $r = 0.9$ if $x < 0.15$ and $r = 1/0.9$ if $x > 0.15$. The density, momentum and energy profiles are displayed in Figures 19, 20 and 21. When looking at the density profile obtained with the HLL scheme, the second Noh artifact is clearly visible, while it does not appear with all the anti-diffusive schemes. This shows the interest in working with anti-diffusive schemes when irregular meshes have to be considered. One also notices that the wall heating

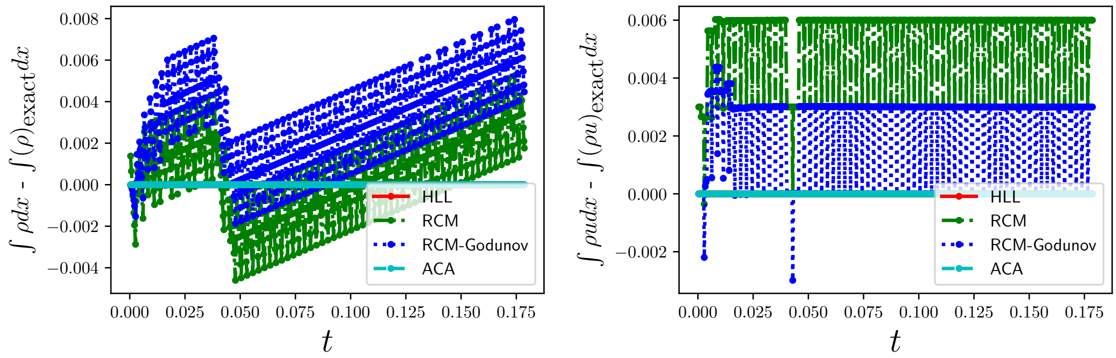

Fig. 18 Isolated weak shock wave: density (left) and momentum (right) time conservation.

is greatly reduced with the anti-diffusive schemes.

B. Noh problem

The second numerical test case we consider is known as the Noh problem. It is similar to the previous test case but the pressure jump is now infinite. The resulting shock created is particularly strong and therefore challenging capturing. The initial conditions are the following

$$\begin{cases} \rho(t=0,x) = 1, \\ u(t=0,x) = -1, \\ \rho e(t=0,x) = 0.5 + 1.5 \cdot 10^{-10}, \end{cases}$$

and $\gamma = 5/3$ so that the initial pressure is $P = 10^{-10}$. The number of cells is 100, the final time $t = 1.2$ and the space domain $[0, 0.6]$.

a. Case of a regular mesh (no geometric progression)

In Figures 23, 24 and 25, the density, momentum and energy profiles are displayed. One notices that the RCM scheme produces strong spurious oscillations while the others remains non-oscillating and accurate. Similarly, to the previous test case the RCM-Godunov and ACA schemes capture the shock waves without any numerical diffusion. The density and momentum conservation displayed in Figure 26 are similar with those obtained with the previous test case.

b. Case of a mesh with local refinement

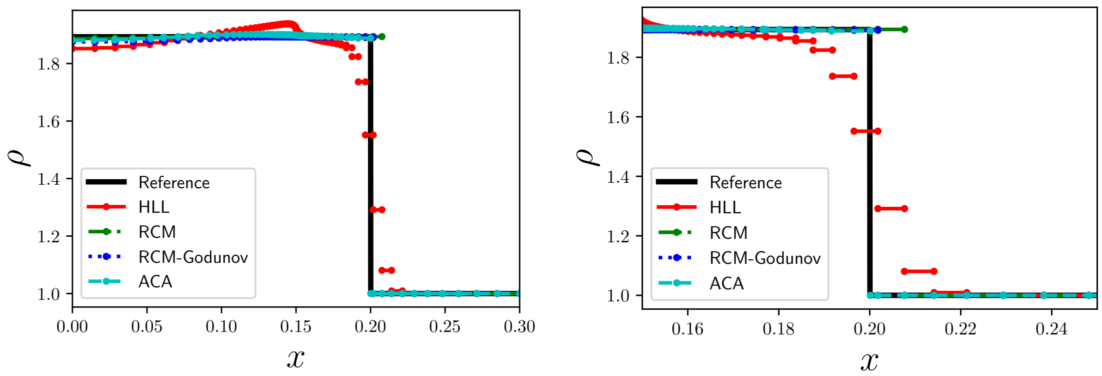

Fig. 19 Isolated weak shock wave on uneven mesh: density profile (left) and zoom on the shock (right).

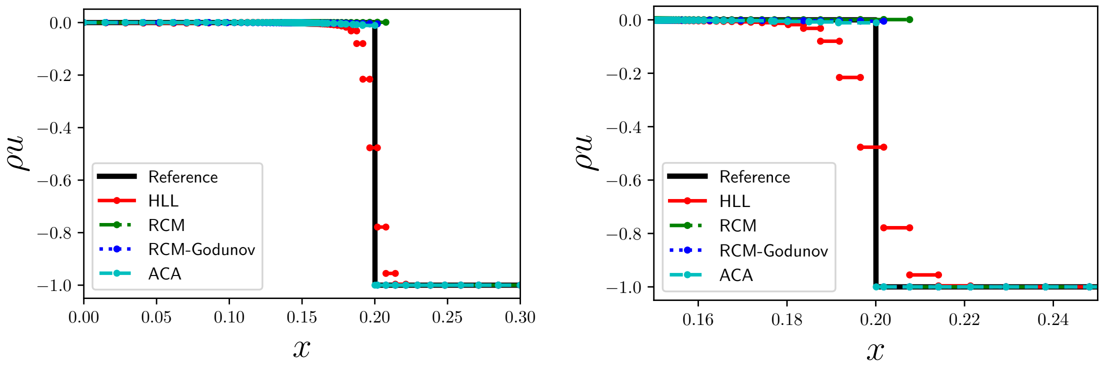

Fig. 20 Isolated weak shock wave on uneven mesh: momentum profile (left) and zoom on the shock (right).

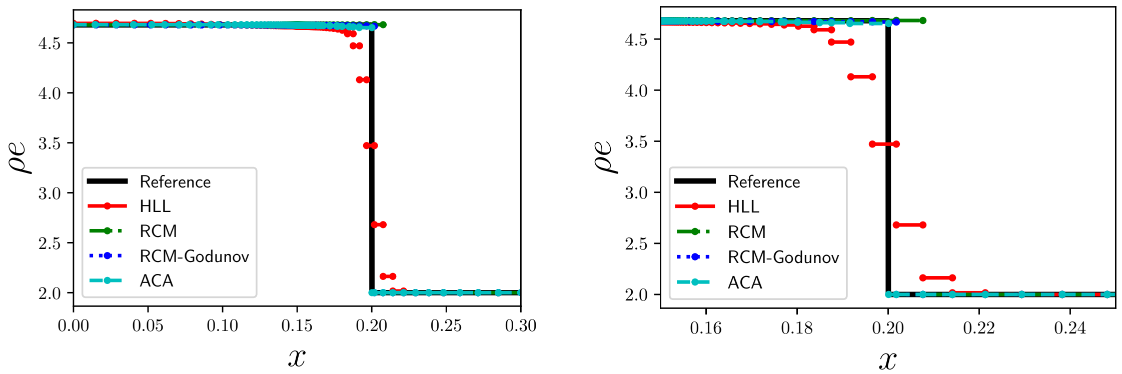

Fig. 21 Isolated weak shock wave on uneven mesh: total energy (left) and zoom on the shock (right).

A progressive mesh is now considered. Here again, we choose $r = 0.9$ if $x < 0.3$ and $r = 1/0.9$ if $x > 0.3$. For clarity, the results obtained with the RCM scheme are not displayed since this scheme is too much oscillatory (see Figure 23). A close look at Figures 28-29 shows that the RCM-Godunov scheme is not perfectly efficient (wrong behaviors are observed when looking at the momentum and energy profiles) while the ACA scheme remains perfectly accurate. The density, momentum and energy profiles are displayed in Figures 27, 28 and 29. When looking at the density profile in Figure 27 obtained with the HLL scheme, the

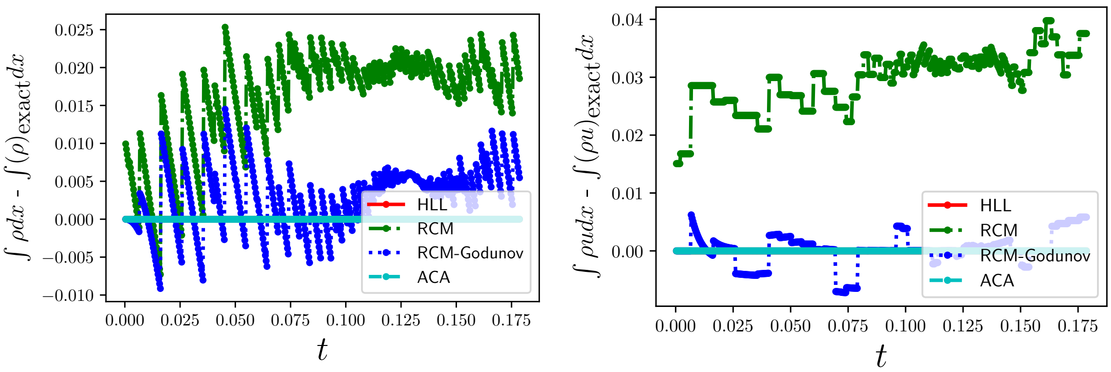

Fig. 22 Isolated weak shock wave on uneven mesh: density (left) and momentum (right) time conservation.

second Noh artifact is clearly visible. Similarly, to the previous test case, it is observed that the second Noh artifacts does not appear with all the anti-diffusive schemes. Here again it is noticed that the wall heating is also greatly reduced when working with the anti-diffusive schemes.

C. Sod problem

The third numerical test case we present is less numerically challenging than the Noh test case (since the shock is moderate) but involves an expansion and a contact discontinuity. It is carried out in order to assess that the anti-diffusive schemes presented herein can be used not only for isolated shock simulations. For this problem, the initial conditions are the following

$$\begin{cases} \rho(t=0,x) = \begin{cases} 1 \ \text{ if } \ x < 0.5, \\ 0.125 \ \text{ if } \ x > 0.5, \end{cases} \\ u(t=0,x) = 0, \\ \rho e(t=0,x) = \begin{cases} 2.5 \ \text{ if } \ x < 0, \\ 0.25 \ \text{ if } \ x > 0. \end{cases} \end{cases}$$

The space domain is $[0,1]$, the number of cell is 100 and the final time $t = 0.2$. In Figure 31, 32 and 33, the density, momentum and energy profiles are displayed at time $t = 0.2$. As expected, all the anti-diffusive schemes correctly capture the right-propagating shock wave while the HLL scheme does not. It is also noticed that the RCM scheme does not behave correctly in the rarefaction wave.

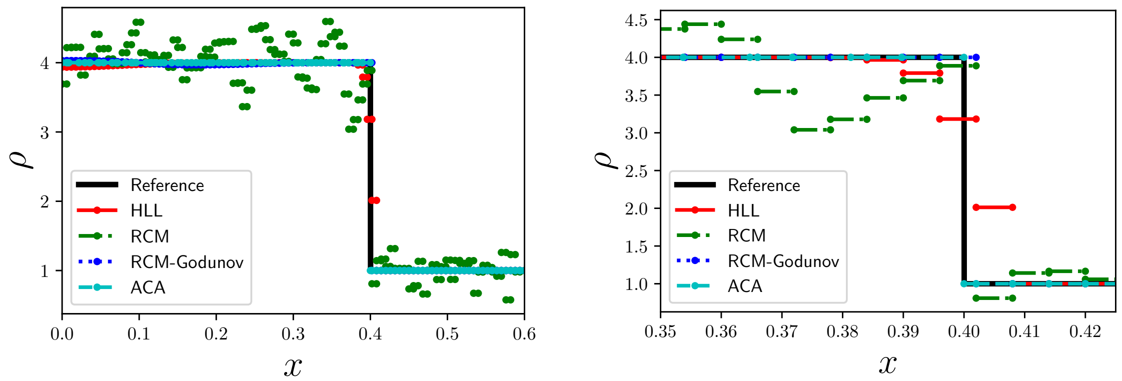

Fig. 23 Noh problem: density profile (left) and zoom on the shock (right).

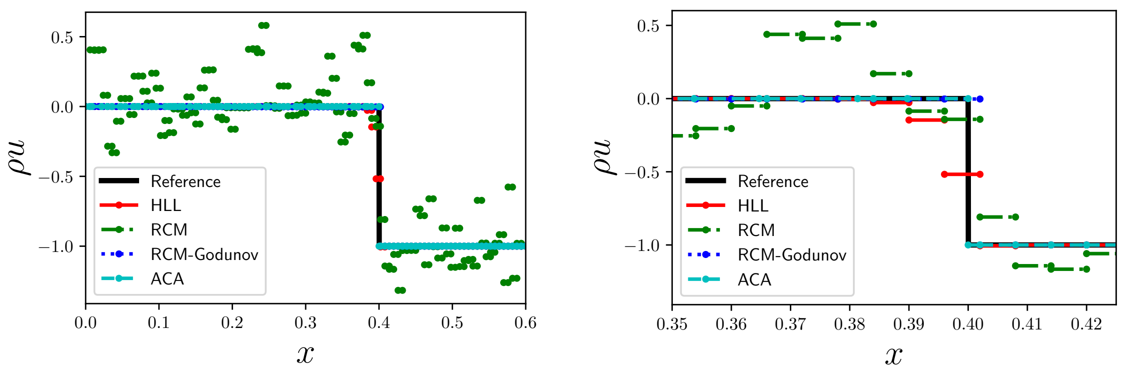

Fig. 24 Noh problem: momentum profile (left) and zoom on the shock (right).

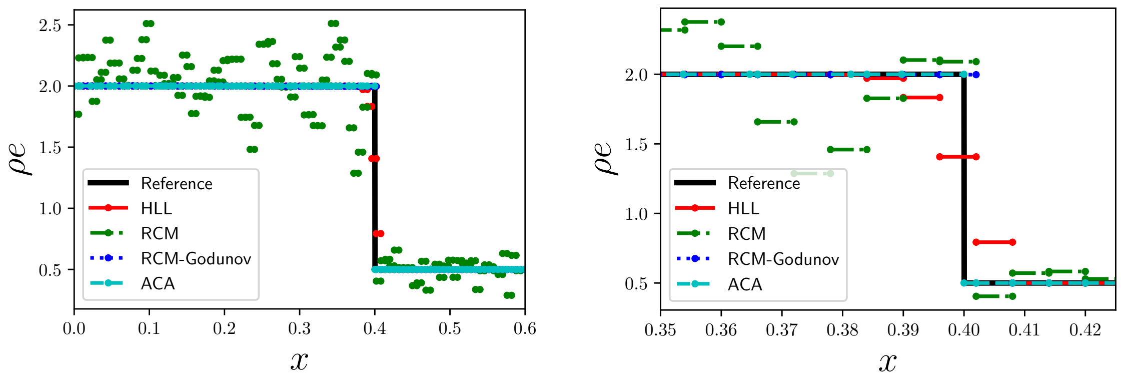

Fig. 25 Noh problem: total energy (left) and zoom on the shock (right).

D. Sedov problem

The fourth and last test case presented is also presented to assess the presented schemes in a non isolated shock context. It consists in the propagation of a strong shock wave directly followed by a rarefaction wave.

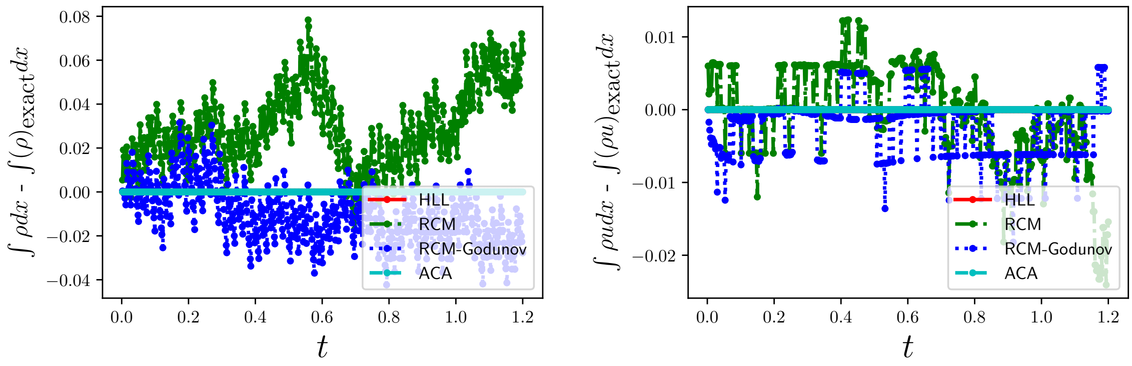

Fig. 26 Noh problem: density (left) and momentum (right) time conservation.

The initial conditions are the following

$$
\begin{cases}
\rho(t=0,x) = 1, \\
u(t=0,x) = 0, \\
\rho e(t=0,x) = \begin{cases} E_0/(2\Delta x) + 1.5 \cdot 10^{-10}, & \text{in the first cell}, \\ 2.5 \cdot 10^{-10}, & \text{otherwise}. \end{cases}
\end{cases}
$$

where $E_0 = 0.134637$ and Δx the size of the first cell (starting form the left side of the domain). This initial condition is a space discretization of a Dirac distribution. The final solutions are displayed at time $t = 1$ using 300 cells and $\gamma = 1/4$. For this problem, it has been observed that the RCM and RCM-Godunov schemes may be very inaccurate and completely miss the correct shock speed. More precisely, it has been observed, for these two schemes, that a slight change in the number of cells produces strong numerical result variations. Also, in Figure 37, large inaccuracy in the total conservations are observed for these two schemes. In addition, the ACA scheme is more accurate than the HLL scheme.

V. Conclusion, limitations and perspectives

In a simple one dimensional framework it has been shown that standard Godunov-type solvers fail in capturing isolated shock waves on meshes with local refinement. This numerical artifact, enlightened by Noh [20], is related to the variation of the numerical viscosity as the cell sizes vary. It has been explained that this artifact, in the context of strong shock simulation in uneven meshes, may be understood as a loss of Rankine-Hugoniot relation which leads to bad plateau prediction. To tackle this numerical problem, several anti-diffusive strategies have been presented and compared with several numerical experiments. In

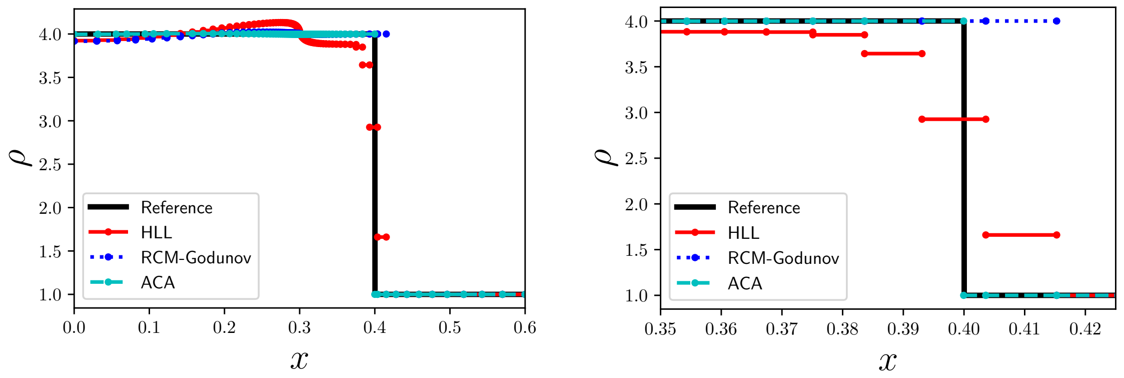

Fig. 27 Noh problem on uneven mesh: density profile (left) and zoom on the shock (right).

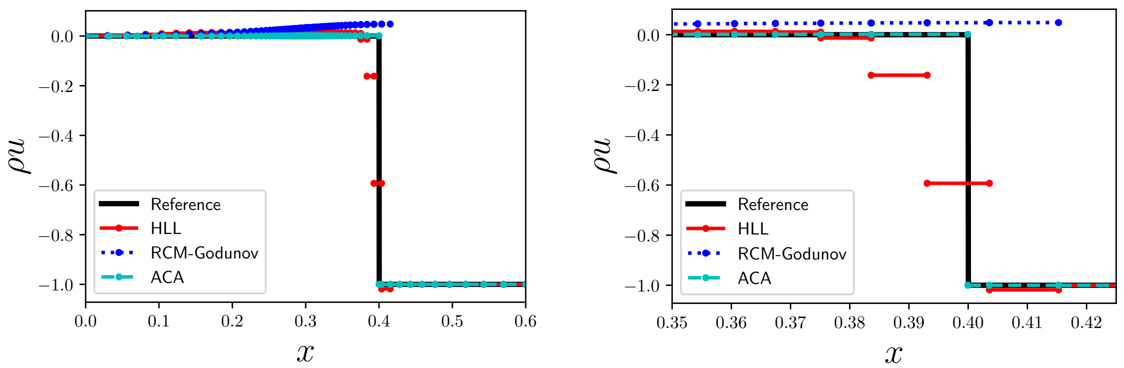

Fig. 28 Noh problem on uneven mesh: momentum profile (left) and zoom on the shock (right).

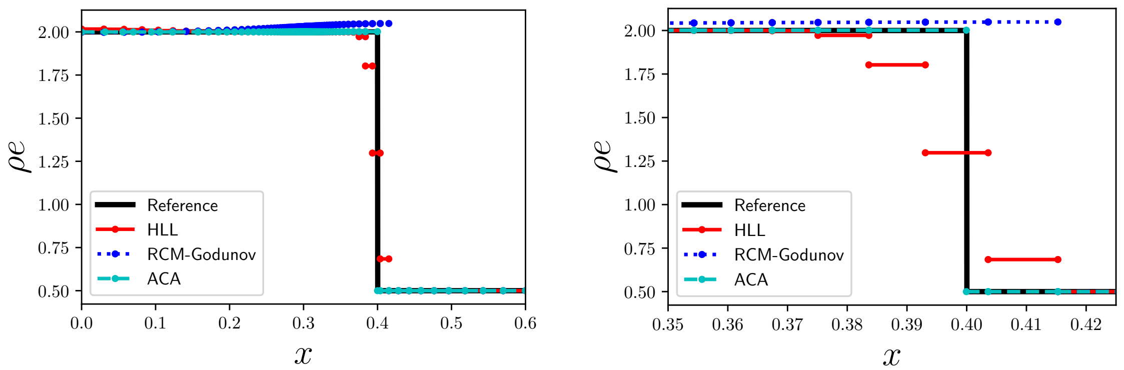

Fig. 29 Noh problem on uneven mesh: total energy profile (left) and zoom on the shock (right).

these approaches inspired by Glimm [13], contrarily to standard Godunov schemes, averages along shock interfaces are avoided such that an isolated shock remains on one cell and is not diffused. For the simulation of weak shocks, all of anti-diffusive techniques presented here allow to address the artifact while they remain numerically stable. However, this study tends to show that anti-diffusive schemes need to be conservative for dealing with strong shock, for both reasons of stability and convergence to the correct shock velocity. This motivates the development of an Anti-diffusive and Conservative ALE-Godunov (ACA) method. We

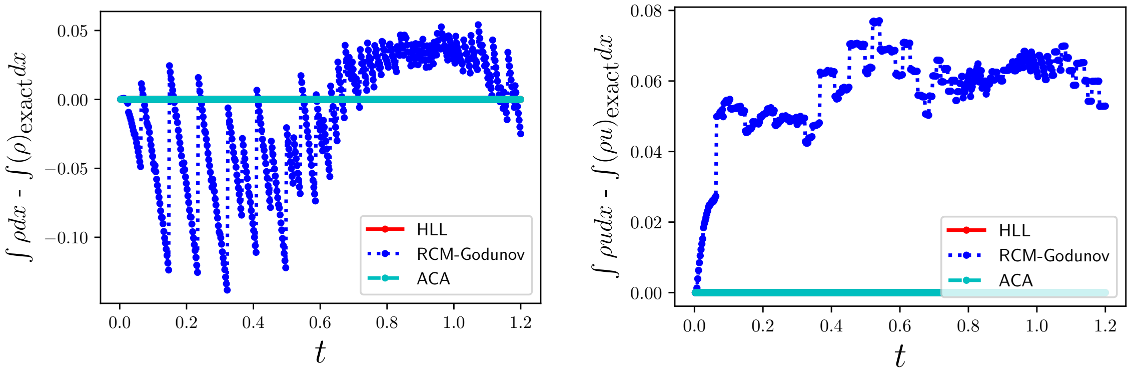

Fig. 30 Noh problem on uneven mesh: density (left) and momentum (right) time conservation.

emphasize that in addition to being conservative, this scheme does not include a random (or pseudo-random) pick-up step, but it needs to displace the mesh at the shock velocity and to remap as the cells become too small. Despite this scheme has been constructed in the sake of exactly capturing isolated shocks, it has been shown that it can be used in other contexts; in the expansion wave or contact discontinuities, ACA behavior is similar to HLL while it allows ensuring sharp shocks. We also mention that anti-diffusive strategies based on discontinuous reconstruction strategies have also been developed in the context of scalar advection problem, downwind decentering procedures [3, 11, 15], capture of contact discontinuities in [2, 10, 17], and capture of isolated shock waves [1, 4]. Even if these procedures are not considered herein, we believe they may also be used to develop anti-diffusive schemes tackling the second Noh artifact since they do not involve numerical diffusion. Various perspectives may be considered here. Firstly, it would be interesting to extend the new anti-diffusive strategy introduced here (ACA scheme) to two-dimensional configurations. However, it is worth noticing that the shock detection and the moving mesh procedure seem particularly challenging extending in 2D. In addition, the methodology presented here strongly relies on the knowledge of the exact shock speed. It would be interesting to extend the methodology to general closure relations by using an approximated shock velocity instead of the exact one (Roe velocity) we use for perfect gas.

[1] N. Aguillon. A non-dissipative reconstruction scheme for the compressible Euler equations. arXiv:1403.7457.

[2] F. Alouges, F. de Vuyst, G. Le Coq, and E. Lorin. The reservoir technique: a way to make Godunov-type schemes zero or very low diffuse. Application to Collela-Glaz solver. Eur. J. Mech. B. Fluids, 27(6):643-664 (2008).

[3] F. Bouchut. An antidiffusive entropy scheme for monotone scalar conservations laws. J. Sci. Comput., 21(1):1-30 (2004).

[4] C. Chalons and N. Aguillon. Non diffusive conservative schemes based on approximate Riemann solvers for

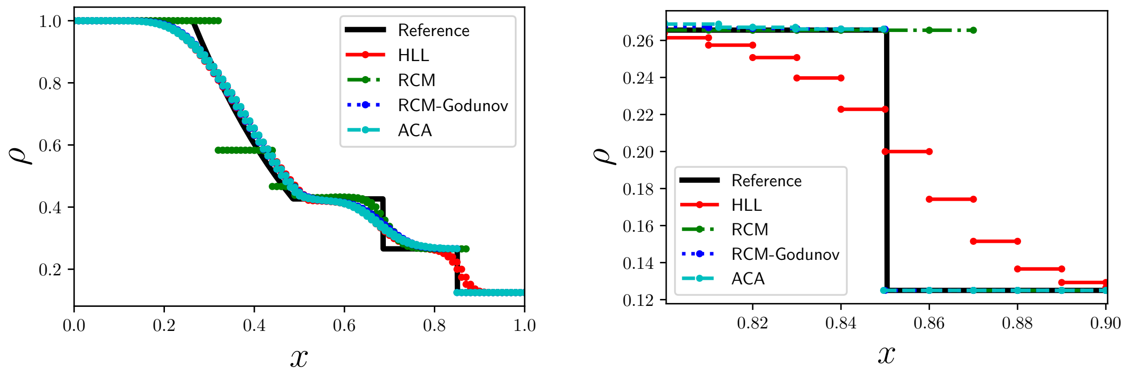

Fig. 31 Sod problem: density profile at final time in the full domain (left) and zoom on the shock (right).

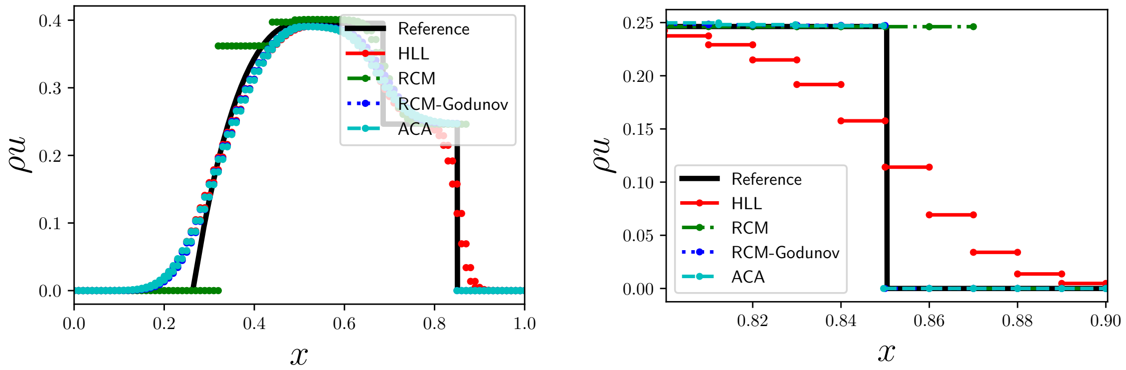

Fig. 32 Sod problem: momentum profile at final time in the full domain (left) and zoom on the shock (right).

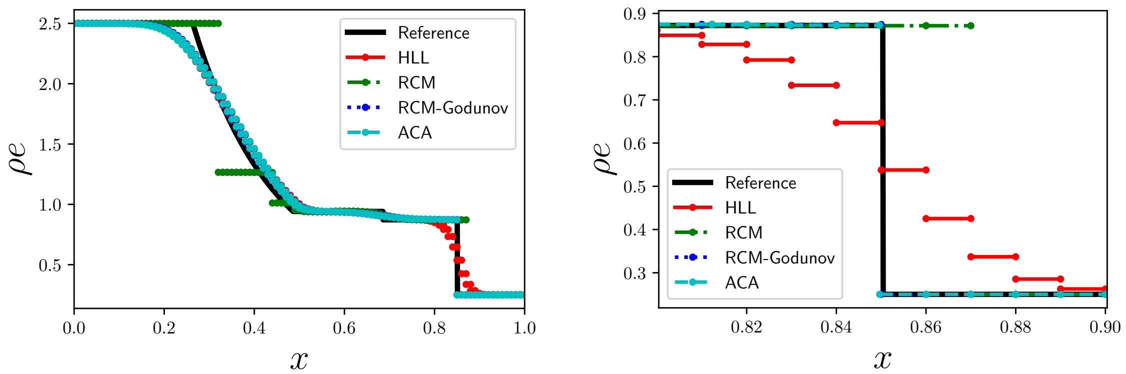

Fig. 33 Sod problem: total energy profile at final time in the full domain (left) and zoom on the shock (right).

Lagrangian gas dynamics. Mathematical modelling and Numerical analysis (M2AN), (2019).

[5] C. Chalons, R. Devigneau, and C. Fiorini. Sensitivity equation method for Euler equations in presence of shocks applied to uncertainty quantification. Phd Thesis 2018.

[6] C. Chalons and P. Goatin. Godunov scheme and sampling technique for computing phase transitions in traffic flow modeling. Interfaces and Free Boundaries, 10(2):197-221, 2018.

[7] A.J. Chorin. Random Choice Solutions of Hyperbolic Systems. J. Comput. Phys. 2:12-26 (1967).

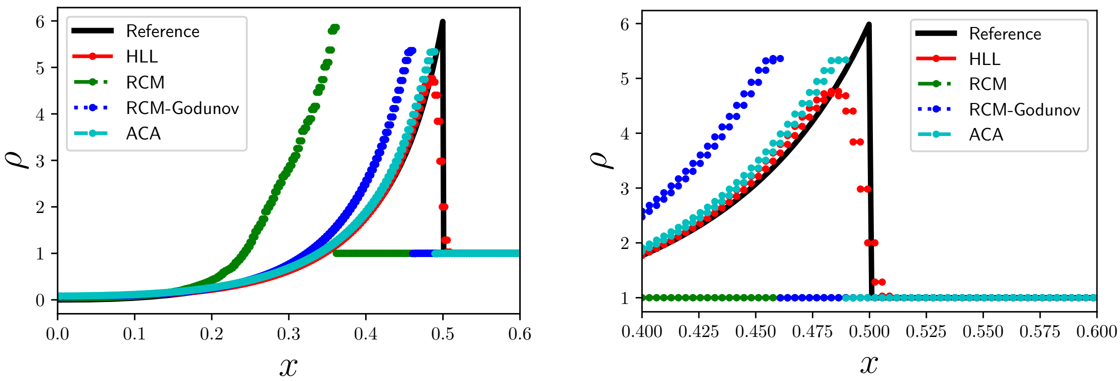

Fig. 34 Sedov problem: density profile at final time in the full domain (left) and zoom on the shock (right).

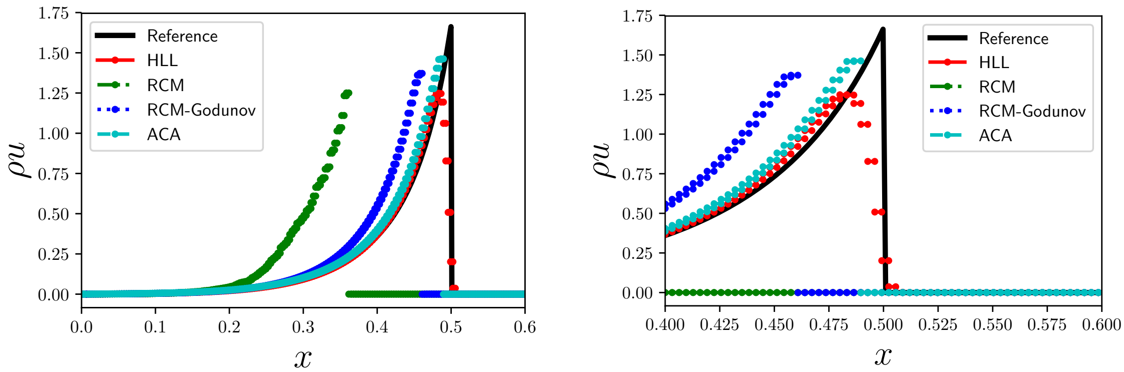

Fig. 35 Sedov problem: momentum profile at final time in the full domain (left) and zoom on the shock (right).

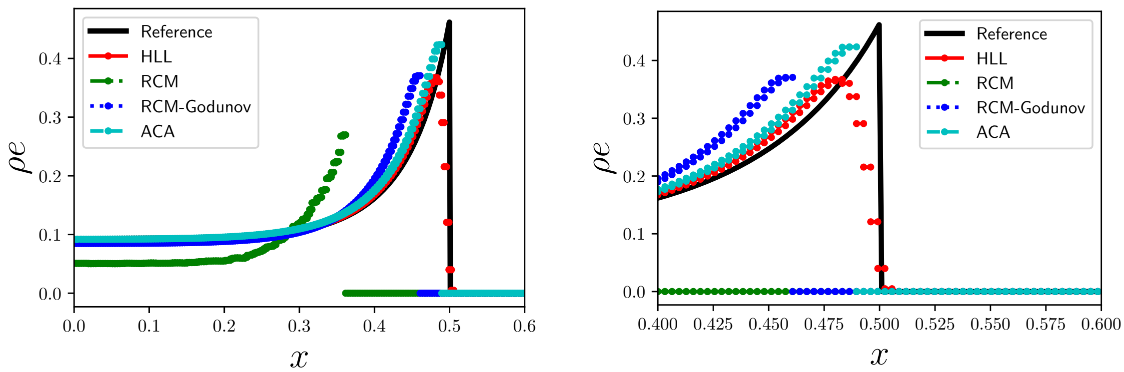

Fig. 36 Sedov problem: total energy profile at final time in the full domain (left) and zoom on the shock (right).

[8] P. Colella. An Analysis of the Effect of Operator Splititng and of the Sampling Procedure on the Accuracy of the Glimm's Method. PhD thesis, Department of Mathematics, University of California, USA, 1978.

[9] P. Colella. Glimm's Method for Gas dynamics. SIAM J. Sci. Stat. Comput., 3(1):76-110, 1982.

[10] J. Sci. Comput. Contact discontinuity capturing schemes for linear advection and compressible gas dynamics. 16(4):479-524 (2002).

[11] B. Despres and F. Lagoutiere. Contact discontinuity capturing schemes for linear advection and compressible gas

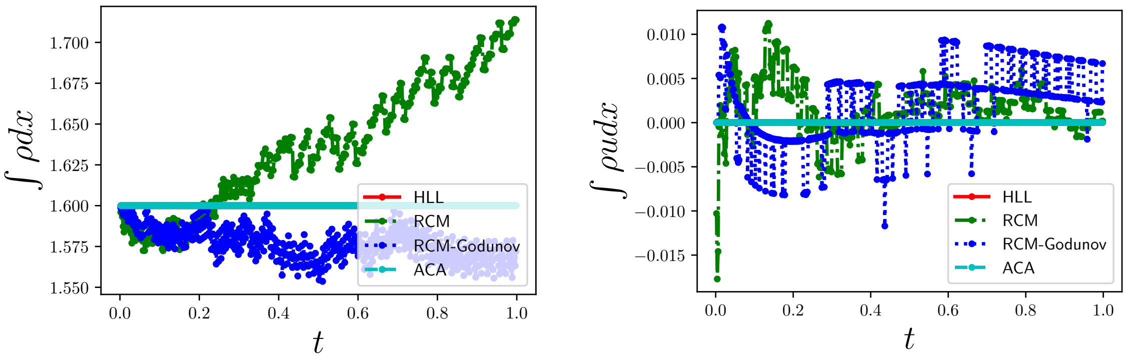

Fig. 37 Sedov problem: mass (left) and momentum (right) conservation during the computation.

dynamics. J. Sci. Comput. 16(4):479-524 (2002).

[12] C. Fiorini. Sensitivity anlysis for nonlinear hyperbolic systems of conservations laws. Phd Thesis 2018.

[13] J. Glimm. Solution in the Large for Nonlinear Hyperbolic System of Equations. Comm. Pure. Appl. Math. 18:697-715, 1965.

[14] A. Harten, P.D. Lax, and B. Van Leer. On upstream differencing and Godunov-type schemes for hyperbolic conservation laws. SIAM Review 25 (1983), 35-61.

[15] F. Lagoutiere. Stability of reconstruction schemes for scalar hyperbolic conservation laws. Commun. Math. Sci. 6(1):57-70 (2008).

[16] R.J. Leveque. Finite volume methods for hyperbolic problems. Cambridge texts in applied mathematics.

[17] Hongxia Li, Zhigang Wang, and De kang Mao. Numerically neither dissipative nor compressive scheme for linear advection and its application to the Euelr system. J. Sci. Comput. 36(3):285-331 (2008).

[18] R. Menikoff. Errors when shock waves interact due to numerical shock width. SIAM J. Sci. Comput. 5 (1994), 1227-1242.

[19] R. Menikoff and K.S. Lackner. Anomalous physical effects from artificial numerical length scales. Report LA-UR-95-2135 (1995).

[20] W.F. Noh. Errors for Calculations of Strong Shocks Using an Artificial Viscosity and an Artificial Heat Flux. J. Comput. Phys. 72, 78-120 (1978).

[21] J.J. Quirk. A contribution to the great Riemann solver debate. Nasa Report (1992).

[22] P.L Roe. Approximate Riemann solvers, parameter vectors, and difference schemes. J. Comput. Phys., 43 (1981), pp.357-372.

[23] P.L Roe. Characteristic-based schemes for the Euler equations. Ann. Rev. Fluid Mech., (1986).

[24] E.F. Toro. Riemann solvers and numerical mehods for fluid dynamics: a practical introduction. Springer Science Business Media, 2013.